High-Temperature Kinetics of the Homogeneous Reverse Water–Gas Shift Reaction

F. Bustamante and R. M. Enick
National Energy Technology Laboratory–Research Associates, Department of Chemical and Petroleum Engineering, University of Pittsburgh, Pittsburgh, PA 15261

A.V. Cugini, R. P. Killmeyer, B. H. Howard, and K. S. Rothenberger
U.S. Department of Energy, National Energy Technology Laboratory, Pittsburgh, PA 15236

M. V. Ciocco and B. D. Morreale
National Energy Technology Laboratory–Support Contractors, Parsons Project Services Incorporated, Library, PA 15129

S. Chattopadhyay
Department of Chemical and Petroleum Engineering, University of Pittsburgh, Pittsburgh, PA 15261

S. Shi
Fluent Incorporated, Morgantown, WV 26505

DOI 10.1002/aic.10099
Published online in Wiley InterScience (www.interscience.wiley.com).

The high-temperature rate of reaction of the homogeneous, reverse water–gas shift reaction (rWGSR) has been evaluated in quartz reactors with rapid feed preheating under both low- and high-pressure conditions. The form of the power-law rate expression was consistent with the Bradford mechanism. The Arrhenius expressions for the reaction rate constant, corresponding to the empty reactor, were in very good agreement with the low-pressure results of Graven and Long, but yielded rate constants roughly four times greater than those obtained in our packed reactor and those reported by Kochubei and Moin and by Tingey. Reactor geometry was not responsible for these differences because computational fluid dynamics simulations revealed similar residence time distributions and comparable conversions when the same kinetic expression was used to model the rWGSR in each reactor. Most likely, the empty NETL reactor and the Graven and Long reactor did not attain an invariant value of the concentration of the chain carrier (H) at low reaction times, which led to an overestimation of the rate constant. Conversions attained in an Inconel® 600 reactor operating at comparable conditions were approximately two orders of magnitude greater than those realized in the quartz reactor. This dramatic increase in conversion suggests that the Inconel® 600 surfaces, which were depleted of nickel during the reaction, catalyzed the rWGSR. *AIChE J,* 50: 1028–1041, 2004
Keywords: water–gas shift, kinetics, homogeneous, high-temperature, Inconel

Introduction

The water–gas shift reaction

The water–gas shift reaction, Eq. 1, is important as a method for further enhancing the yield of hydrogen from industrial processes such as the steam reforming of natural gas or the gasification of heavy carbonaceous materials. Syngas mixtures containing mostly hydrogen and carbon monoxide are typically generated at elevated temperatures via the conversion of natural gas, coal, biomass, petroleum, and organic wastes (Wender, 1996). Steam is then added to the CO–H_2 feed mixture before being introduced to water–gas shift (WGS) reactors to convert the CO to CO_2 and additional H_2. However, thermodynamic equilibrium favors high conversion of CO and steam to hydrogen and carbon dioxide at low temperatures. Therefore, the

Correspondence concerning this article should be addressed to F. Bustamante at fbustamu@udea.edu.co.

water–gas shift reaction is commonly conducted at low temperature in the presence of catalysts that enhance the reaction rate.

$$CO + H_2O \leftrightarrow CO_2 + H_2 \qquad \Delta H = -41 \text{ kJ/mol} \qquad (1)$$

The water–gas shift reaction is reversible and several correlations for the equilibrium constant have been published (Babieri and DiMaio, 1997; Benson, 1981; Moe, 1962; Singh and Saraf, 1977). A simple temperature-dependent correlation (Moe, 1962) was used to estimate K_{eq} in this study.

$$K_{eq} = \exp\left\{-4.33 + \frac{4577.8}{T}\right\} \qquad (2)$$

There are numerous kinetic studies of the catalyzed forward water–gas shift reaction at temperatures up to 873 K (Newsome, 1980). Kinetic studies of the forward or reverse water–gas shift reaction at elevated temperatures (>873 K) are uncommon, however. This scarcity of data is probably attributable to the low equilibrium conversions of CO that can be achieved in conventional reactors operating in this temperature range. High conversions at elevated temperature can be achieved in a hydrogen-permeable membrane reactor, however (Enick et al., 2000). Further, extreme temperatures could enhance the kinetics to the extent that the reaction would proceed rapidly in the absence of heterogeneous catalysts. Therefore, an understanding of the forward and reverse reaction rates would be useful in the design of high-temperature, hydrogen-permeable membrane reactors. The *reverse* water–gas shift reaction (rWGSR) is the focus of this investigation.

The reverse water–gas shift reaction

Several investigations of the high-temperature (>1148 K), low-pressure (<0.101 MPa), homogeneous, uncatalyzed rWGSR have been conducted. Power-law correlations that comply with the Bradford mechanism (Bradford, 1933), a simple gas-phase chain-reaction model, have been used to model the rate of reaction. Although models based on a more comprehensive network of elementary steps, such as a model for the oxidation of H_2 and CO in sub- and supercritical water (Holgate and Tester, 1994), could be used to describe the reaction, we have found that such a network yields results nearly identical to the Bradford mechanism. Therefore, the Bradford mechanism was considered to be an adequate representation of the rWGSR under the conditions studied.

The Bradford mechanism, provided below, employs M as any gas-phase molecule:

$$H_2 + M \xrightarrow{k_1} 2H + M \qquad \text{Dissociation of hydrogen} \qquad (3)$$

$$H + CO_2 \underset{k_{-2}}{\overset{k_2}{\longleftrightarrow}} CO + OH \qquad \text{Reaction between H and } CO_2 \qquad (4)$$

$$OH + H_2 \underset{k_{-3}}{\overset{k_3}{\longleftrightarrow}} H_2O + H \qquad \text{Reaction between OH and } H_2 \qquad (5)$$

$$M + 2H \xrightarrow{k_{-1}} M + H_2 \qquad \text{Reassociation of hydrogen} \qquad (6)$$

It has been shown (Graven and Long, 1954; Tingey, 1966) that the condition of low conversion (i.e., negligible effect of the opposing reaction) and the assumption of a stationary state for the concentrations of the intermediates (H and OH concentrations do not change significantly with respect to time) leads to the following rate expression:

$$r = \frac{d[CO]}{dt} = \left(\frac{k_1}{k_{-1}}\right)^{0.5} k_2[H_2]^{0.5}[CO_2] \qquad (7)$$

Accordingly, the rate constant for the rWGSR may be expressed as

$$k = \left(\frac{k_1}{k_{-1}}\right)^{0.5} k_2 \qquad (8)$$

Therefore, the expression for the rate of reaction in terms of k becomes

$$r = \frac{d[CO]}{dt} = k[H_2]^{0.5}[CO_2] \qquad (9)$$

The temperature dependency of the rate constant k is described by the Arrhenius equation

$$k = k_0 e^{-E_a/RT} \qquad (10)$$

Most prior investigations of the homogeneous rWGSR at elevated temperature have used power law models that are consistent with Eqs. 9 and 10. The activation energy and pre-exponential constant associated with each of these studies are summarized in Table 1. Graven and Long (1954) studied the rWGSR in the temperature range 1148–1323 K. CO_2 and H_2 were introduced to the reactor along with the N_2 diluent gas to control partial pressures. Their cylindrical quartz reactor (3.4 cm diameter, 6.4 cm length) featured tangential feed and withdrawal lines (1.5 mm ID). They reported that the reaction occurred rapidly in the gas phase without any heterogeneous contribution from the quartz surfaces. Tingey's reactor (Tingey, 1966) consisted of a cylindrical quartz tube (3.3 cm ID, 27.1 cm length) that contained a coaxial quartz insert (2.2 cm ID, 21.0 cm length), resulting in a long annular flow section that was preceded and followed by short cylindrical sections (3.3 cm ID, 6.1 cm combined length). Coaxial capillary tubing served as feed and effluent channels for the reactor. Kochubei and Moin (1969) designed empty quartz reactors (ID ranging from 0.6 to 6.5 cm) that used a static mixer to mix the preheated hydrogen and carbon dioxide. The effluent gases were withdrawn from a capillary tube (1.5 mm ID), extending in the same axial direction as the cylinder, but located along the

Table 1. Kinetic Expressions for the rWGSR in Quartz Reactors*

Reference	T (K)	p (MPa)	α	β	E_a (kJ/mol)	k_0 (L/mol)$^{\alpha+\beta-1}$ s^{-1}
Graven and Long (1954)	1148–1323	0.1	0.5	1.0	234.3	2.9×10^{9}
Kochubei and Moin (1969)	1023–1523	0.1	0.5	1.0	326.4	6.4×10^{12}
Tingey (1966)	1073–1323	0.1	0.5	1.0	318.0	1.2×10^{13}
Tingey (1966)	673–1073	0.1	0.333	1.0	164.2	7.6×10^{4}
Karim and Mohindra (1974)	<2500	0.1	0.5	1.0	397.5	2.3×10^{16}
NETL empty reactor (this work)	1148–1198	0.1	0.5	1.0	222.2 ± 3.9	1.09×10^{7}
NETL empty reactor (this work)	1148–1198	1.6	0.5	1.0	218.4 ± 5.1	5.99×10^{8}
NETL packed reactor (this work)	1063–1138	1.6	0.5	1.0	355.6 ± 1.5	3.0×10^{14}

*$r = k[H_2]^{\alpha}[CO_2]^{\beta} = k_0\exp(-Ea/RT)[H_2]^{\alpha}[CO_2]^{\beta}$, $R = 8.3145 \times 10^{-3}$ kJ/mol · K.

outside edge of the reactor. Tingey (1966) and Kochubei and Moin (1969) published results that were in very good agreement, with both obtaining lower values for the rate of reaction than those obtained by Graven and Long (1954). Tingey suggested that the higher reaction rate reported by Graven and Long (1954) may have been caused by traces of oxygen in their feed stream that acted as a homogeneous catalyst, but was unable to substantiate this claim.

The values of the rate constant k, for the low-pressure rWGSR, are presented as a function of inverse absolute temperature over the 1123–1223 K in Figure 1. The pre-exponential constant and activation energy of each correlation is listed in Table 1. The prediction of the Karim and Mohindra (1974) model of the water–gas shift reaction as twelve, simple, reversible, intermediate reaction steps involving nine species at temperatures up to 2500 K, which used kinetic data available at the time is also presented. Given the disagreement among these reported values, our first objective was to investigate the rWGSR kinetics at low-pressure conditions in quartz reactors. The rWGSR kinetics were then determined in a pressure-equilibrated quartz reactor that enabled the reaction to be conducted at elevated pressures similar to those attained in a gasifier. Finally, the rWGSR was conducted in an Inconel® 600 vessel at both low- and high-pressure conditions to assess the catalytic influence of the metal reactor wall on the reaction rate. The reactors were designed to be analogous to the industrial application: rapid heating of a hydrogen and carbon dioxide gas mixture followed by introduction to the quartz or Inconel® 600 reactor. In all cases, only the reacting gases, CO_2 and H_2, were introduced to the reactor. Gas-phase partial pressures were adjusted by varying both total pressure and feed composition.

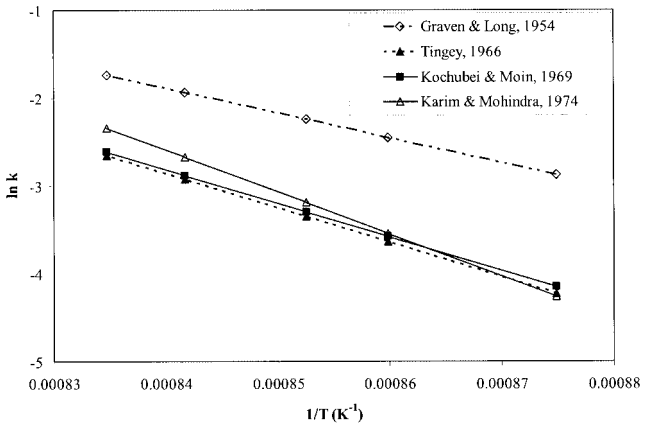

Figure 1. Arrhenius representations of rate constant expressions for the reverse water–gas shift reaction (rWGSR) obtained using a quartz reactor, $r = k[CO_2][H_2]^{0.5}$, k ($L^{0.5}$ $mol^{-0.5}$ s^{-1}); results of previously published literature.

Experimental

rWGSR apparatus

The Hydrogen Membrane Test Unit Number 1 (HMT-1) at the U.S. DOE National Energy Technology Laboratory (NETL) was designed to attain high-pressure (up to 3.0 MPa), high-temperature (up to 1198 K) conditions in Inconel® 600 or quartz reactors (Figure 2). The reaction pressure was controlled with a stainless steel Badger Research pressure control valve (PCV) equipped with a control loop with a pressure indicator (PI). The reaction temperature was controlled with a ceramic resistance heater using a control loop with a coaxially mounted, dual-element type-K thermocouple (TI), which was placed approximately 3 mm from the reactor. An Iconic Genesis process control program provided the process control for the unit. It was not possible to place a thermocouple inside the reactor to monitor the outlet temperature because of the catalytic effect of the metal. The existence of a temperature profile, however, was verified with hydrogen or carbon dioxide flowing through the system. Under typical low-pressure experimental conditions, the temperature within the reaction zone varied by ±8 K along its length from the average temperature that was used in the evaluation of the data.

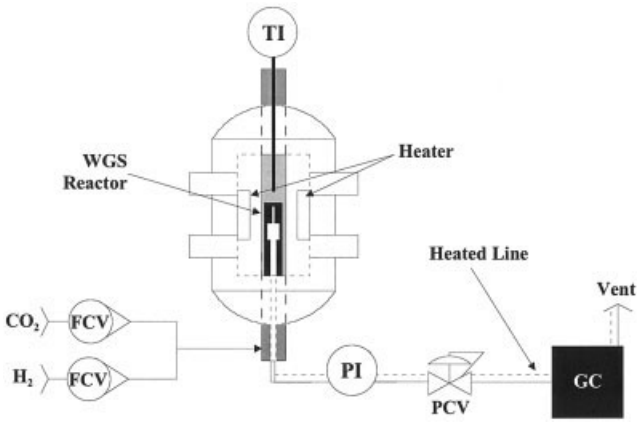

Figure 2. Schematic of HMT-1 unit. FCV, flow control valve; PCV, pressure control valve; PI, pressure indicator; GC, gas chromatograph; TI, temperature indicator.

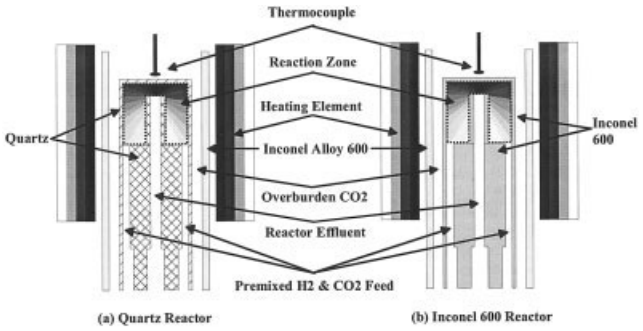

Figure 3. Details of the quartz (a) and Inconel® 600 (b) reactors.

Reactor Feed. The flow rates of the feed gases, H_2 and CO_2 (99.999%), were controlled with Brooks 5850i mass flow controllers (FCVs) and verified with a soapfilm flow meter. Kinetic studies were conducted using either an equimolar feed mixture introduced to the reactor over a range of flow rates or feed mixtures in which the concentration of one reactant was held constant while the concentration of the other was varied. Partial pressures were established by adjusting feed gas composition and total pressure; no inert diluent gases were used. An oxygen trap was located in front of the reactor to eliminate the pronounced catalytic influence of O_2 on the reaction. Concentrations of oxygen in the feed remained below the gas chromatograph detection limit of 1 ppm.

The reactants were premixed and then fed to the quartz reactor through quartz tubing and a narrow annulus with a volume of 0.2 cm^3, approximately one tenth that of the reaction zone volume. The gases were rapidly heated from 873 K to the reaction temperature as they passed through the annulus (annular gap = 0.13 mm). Control experiments indicated that no conversion of the CO_2 in the quartz reactor was detectable for reaction temperatures below 873 K.

Reaction Zone. A pressure-equilibrated quartz reactor or Inconel® 600 reactor was accommodated in the HMT-1 unit. The geometry of these reactors is illustrated in Figure 3 and the dimensions of the reaction zone are provided in Table 2. When the quartz reactor was operated at elevated pressure, a pressure equalization fluid, CO_2, was maintained at the same pressure as that of the reacting gases within the reactor to prevent stresses across the reactor walls. The preheated feed gases entered the reaction zone and flowed upward toward the top of the narrow inner tube that led to the reaction zone exit. Residence times of 0.3–0.5 s were chosen for the reactions conducted in the quartz reactor at low pressure. This yielded conversions of 0.1–0.8 %, which were great enough to ensure accurate calculation of conversion. Residence times of 2–10 s were realized at high-pressure conditions because of the increased gas density. Comparable residence times were selected when the Inconel® 600 reactor was used.

The reacting gases then flowed downward through the inner tube and exited the reaction zone. The reaction products were rapidly cooled to 873 K as they flowed toward the reactor effluent line. The temperature of the tubing was maintained at 573–673 K, which was hot enough to prevent condensation of water produced by the rWGSR but cold enough to prevent further conversion of the reactants.

Effluent Gas Stream. The effluent of the reactor was analyzed with a gas chromatograph equipped with a TCD detector. Argon was used as carrier gas. The GC column, HayeSep® D (porous polymer), allowed the separation and quantification of H_2, CO, CO_2, and H_2O in the range of concentrations of interest. Concentrations of oxygen in the product remained below the detection limit of 1 ppm. Reaction rates were evaluated from the CO_2 conversion, CO_2 concentration, and residence time. Rates calculated from H_2 were found to be identical. Once the CO_2 and H_2 concentration exponents of the rate expression were elucidated, the rate constant was calculated from the rate value by using the integrated form of a PFR reactor design equation (Fogler, 1999).

Computational fluid dynamics numerical simulations

The steady-state flow of the gases through the empty quartz reactor used in this study was modeled using computational fluid dynamics (CFD). Similar computations were also performed for the reactors described by Graven and Long (1954), Tingey (1966), and Kochubei and Moin (1969). The objective of these computations was to determine whether the reactor geometry could have influenced the kinetic results. Mixing within the reactor was assessed using residence time distribution (RTD) plots that were determined by simulating the effluent concentration of a gas (hydrogen) that was pulsed into the feed stream (nitrogen). Additionally, the rWGSR was modeled in each reactor under the same conditions of temperature, pressure, residence time, and rate constant expression, to elucidate the effect of the nonideal flow on the kinetic results. A commercial CFD software (Fluent, 2003), was used for all the numerical simulations.

Flow Field. The geometries were generated and meshed by using Gambit 2.0 software (Fluent). Axisymmetric two-dimensional geometries that incorporated a mesh of quads were used for the NETL quartz reactor and the Tingey (1966) reactor. Three-dimensional geometries that incorporated a mesh of hexahedral/tetrahedral hybrid grids were used for the Graven and Long (1954) reactor and the Kochubei and Moin (1969) reactor. Finer grids were applied at the reactor inlet, reactor outlet, and near the reactor walls in all cases.

The governing equations that were solved to describe the flow of gas through the isothermal reactors consisted of the continuity equation and the Navier–Stokes equations. The continuity equation can be expressed in the following form:

$$\frac{\partial \rho}{\partial t} + \nabla.(\rho \vec{v}) = 0 \qquad (11)$$

Table 2. Dimensions of the Reaction Zone of the NETL Quartz and Inconel® 600 Reactors

Parameter	Quartz with Tube*	Inconel with Tube
Reactor height (cm)	1.9	2.54
Reactor ID (cm)	1.1	1.35
Inner tube height (cm)	1.4	1.91
Inner tube ID (mm)	1.85	2.87
Inner tube OD (mm)	3.85	4.14
Annular gap, reactor (mm)	3.57	4.66
Volume (cm^3)	1.81	3.38

*Quartz packing (small rods, 2 mm diameter, 3 mm long) was added to the quartz reactor in some experiments.

where ρ is the density, t is time, and $\vec{v}$ is the velocity vector. The conservation of momentum equation is described as

$$\frac{\partial}{\partial t}(\rho\vec{v}) + \nabla.(\rho\vec{v}\vec{v}) = -\nabla p + \nabla.(\bar{\bar{\tau}}) \tag{12}$$

where p is the pressure and $\bar{\bar{\tau}}$ is the stress tensor given by

$$\bar{\bar{\tau}} = \mu\left[(\nabla\vec{v} + \nabla\vec{v}^{\mathbf{T}}) - \frac{2}{3}\nabla.\vec{v}I\right] \tag{13}$$

where μ is the molecular viscosity, I is the unit tensor, the superscript **T** means transposed matrix, and the second term on the right-hand side is the effect of volume dilation. Because the flow is laminar in the reactors, no turbulence model has been included.

For steady-state calculations, the time derivative terms vanished. The governing equations were discretized by using a control-volume technique in which the algebraic equations were integrated on each control volume, yielding discrete equations that conserved each quantity on a control-volume basis. Second-order upwind schemes were used for spatial discretizations. The solutions were converged quickly and the residuals were kept under 1.0E-06.

Simulation of a Tracer Input. This simulation is an unsteady-state calculation, and thus time derivative terms were included. A first-order implicit method was applied to discretize the governing equations. In this simulation, the species transport scalar equations were solved to trace the evolution of the species. The species transport scalar equation can be written in the following form:

$$\frac{\partial}{\partial t}(\rho Y_i) + \nabla.(\rho\vec{v}Y_i) = -\nabla.\vec{J}_i + R_i + S_i \tag{14}$$

where Y_i is the local mass fraction of species i, $\vec{J}_i$ is the diffusion flux of species i, R_i is the net rate of production of species i by chemical reaction, and S_i is the rate of reaction by addition from the dispersed phase plus any user-defined source.

The diffusion flux of species i was formulated as

$$\vec{J}_i = \rho D_{i,m}\nabla Y_i \tag{15}$$

where $D_{i,m}$ is the diffusion coefficient for species i.

The two components used in the tracer simulation were nonreactive; therefore the last two terms in the species transport equation (Eq. 14) were neglected. The flow rate at the inlet of the reactor was calculated corresponding to a residence time of 0.5 s. The inlet conditions were specified as to simulate a pulse of hydrogen into a stream of nitrogen flowing to the reactor:

- $t \leq 0$ s and $t > 0.01$ s: only N_2 flows into the reactor.
- $0 < t \leq 0.01$ s: a pulse of dilute H_2 (mole fraction = 0.01) is introduced.

Simulation of the Conversions inside the Reactor. When reactions are involved, the net source of chemical species i attributed to reaction R_i in the species transport scalar equation can be computed as the sum of the reaction source over the N_R reactions that the species participates in

$$R_i = M_{w,i}\sum_{r=1}^{N_R}\hat{R}_{i,r} \tag{16}$$

where $M_{w,i}$ is the molecular weight of species i, N_R is the number of the reactions, and $\hat{R}_{i,r}$ is the molar rate of creation/destruction of species i in reaction r.

The molar rate of creation/destruction of species i in reaction r is given by

$$\hat{R}_{i,r} = (v''_{i,r} - v'_{i,r})\left(k_{f,r}\prod_{j=1}^{N_r}[C_{j,r}]^{\eta_{j,r}'} - k_{b,r}\prod_{j=1}^{N_r}[C_{j,r}]^{\eta_{j,r}''}\right) \tag{17}$$

where

$v'_{i,r}$ = stoichiometric coefficient for reactant i in reaction r
$v''_{i,r}$ = stoichiometric coefficient for product i in reaction r
N_r = number of chemical species in reaction r
$C_{j,r}$ = molar concentration of reactant and product species j in reaction r
$\eta'_{j,r}$ = forward rate exponent for each reactant and product species j in reaction r
$\eta''_{j,r}$ = backward rate exponent for each reactant and product species j in reaction r

For the low conversions observed in our study, the rate of reaction can be expressed as Eq. 9. The parameters for the rate constant (Eq. 10) were evaluated by determining the temperature dependency of Eq. 8 using values available from the updated and comprehensive kinetic GRI database (GRI-MECH 3.0, 2000) for each of the elementary reactions. The resultant parameters were $k_0 = 3.52\text{E}{+}11$ $(\text{m}^3/\text{mol})^{0.5}$ s^{-1} and $E_a = 3.27\text{E}{+}05$ (J/mol). The residence time was set at 0.5 s for a stoichiometric feed of hydrogen and carbon dioxide.

Results and Discussion

Low-pressure rWGSR in a quartz reactor

Equimolar feeds of CO_2 and H_2 were introduced at a total pressure of 0.101 MPa to the empty NETL quartz reactor that is illustrated in Figure 3. The power-law exponents of the H_2 and CO_2 were assumed to be 0.5 and 1.0, respectively. The Arrhenius representation of the reaction rate data for this low-pressure rWGSR over the 1148–1198 K temperature range is found in Figure 4. Table 1 provides the corresponding activation energy and pre-exponential constant.

The NETL rWGS reaction rate constant was approximately 20% greater than that reported by Graven and Long (1954), as illustrated in Figure 4. The activation energy of 53.1 ± 0.9 kcal/mol (222.2 ± 3.9 kJ/mol) was slightly less than the value of 56 kcal/mol (234.3 kJ/mol) reported by Graven and Long. The measured reaction rate constant values were roughly four times greater than those reported by Tingey (1966) and Kochubei and Moin (1969), however, as shown in Figures 1 and 4 and Table 1. Thus, our low-pressure results for the empty reactor exhibited closest agreement with the results of Graven and Long (1954).

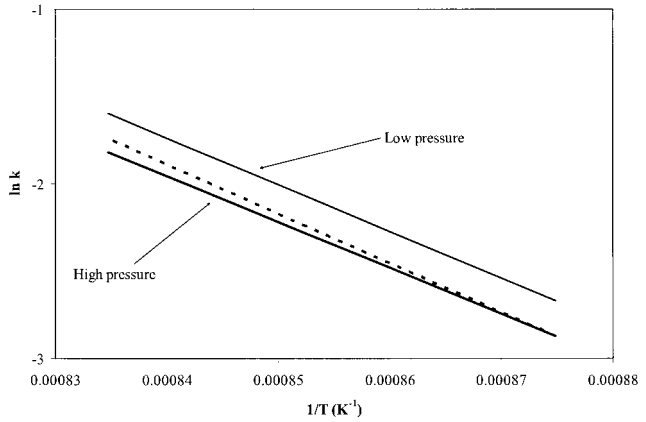

Figure 4. Arrhenius representations of rate constant expressions for the reverse low- and high-pressure WGS reaction obtained at NETL using the quartz reactor, $r = k[CO_2][H_2]^{0.5}$, k ($L^{0.5}$ $mol^{-0.5}$ s^{-1}).

Graven and Long low-pressure correlation (Graven and Long, 1954) (dotted line) provided for reference.

High-pressure rWGSR in a quartz reactor

Equimolar feeds of CO_2 and H_2 were introduced at a total pressure of 1.6 MPa to the NETL empty quartz reactor. A separate stream of a pressure equalization fluid, CO_2, was also maintained at 1.6 MPa in the space between the outer surface of the quartz reactor and the inner wall of the Inconel® 600 pressure vessel. The power-law exponents of the H_2 and CO_2 were determined to be 0.5 and 1.0, respectively (see Figures 5 and 6). The results are summarized in Figure 4 and Table 1. The activation energy of 52.2 ± 1.2 kcal/mol (218.4 ± 5.1 kJ/mol) was slightly smaller than the low-pressure result of 53.1 ± 0.9 kcal/mol (222.2 ± 3.9 kJ/mol) and the reaction rate constant slightly less than that reported by Graven and Long. Thus, our high-pressure results for the empty reactor were also in good agreement with the findings of Graven and Long (1954).

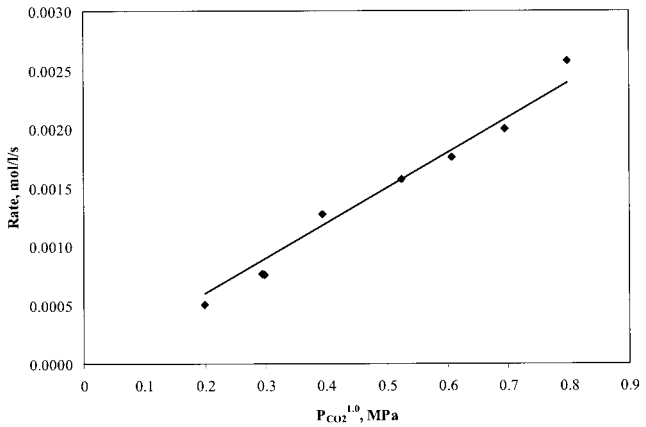

Figure 5. Dependency of the rate on the concentration of CO_2. Partial pressure of H_2 was maintained at 0.8 MPa.

All experiments were performed at 1173 K. Residence time = 1.92 ± 0.15 s based on swept volume.

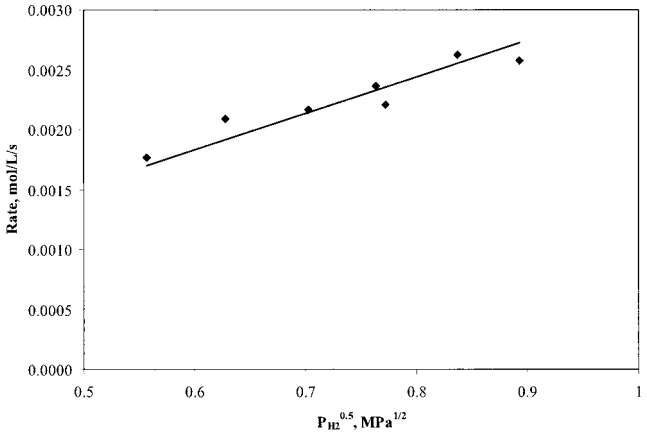

Figure 6. Dependency of the rate on the concentration of H_2. Partial pressure of CO_2 was maintained at 0.8 MPa.

All experiments were performed at 1173 K. Residence time = 1.85 ± 0.08 s based on swept volume.

Effect of reactor geometry on quartz reactor results

An attempt was made to determine the cause of the differences between the low-pressure rate constant correlations illustrated in Figures 1 and 4. Tingey (1966) suggested the relatively high reaction rate constant values reported by Graven and Long (1954) may have been caused by oxygen in their feed stream, but our rate constants derived from the empty quartz reactor were comparable to those of Graven and Long and no detectable amounts of O_2 were found in the CO_2 or H_2 feed streams or the premixed feed stream. Therefore, CFD calculations were performed to determine whether the reactor geometry could have influenced the kinetic results. Comparisons of the flow patterns of a nonreacting gas, the residence time distributions of a nonreacting mixture, and the conversion of the rWGSR under identical conditions were made for the NETL empty quartz reactor and the Graven and Long (1954), Kochubei and Moin (1969), and Tingey (1966) reactors.

Flow Patterns and Residence Time Distributions. In each representation of the flow patterns within the reactor (Figures 7–10), the length of the vector is proportional to the velocity of the particle at the origin of the vector. The direction of the vector indicates the direction in which the fluid located at the origin of the vector is moving. In some cases, as noted in the figure legends, portions of the reactor in which the fluid is moving at extremely high velocity are represented by a white field (rather than a group of extremely long vectors), to avoid cluttering the figure.

The NETL quartz reactor was characterized by upward flow through the large annular gap within the reaction zone followed by a flow reversal at the top of the reactor. The gas then flowed vertically downward through the inner tube. There is a very small stagnant zone above the exiting port. This is manifested in the tailing of the residence time distribution (RTD) plot (Figure 11), which exhibits a distribution broader than that expected for a laminar flow reactor with axial dispersion (Fogler, 1999).

The tangential feed and withdrawal of the Graven and Long reactor induced circular flow that formed vortices within the reactor, as shown by the velocity vectors along the edge of the

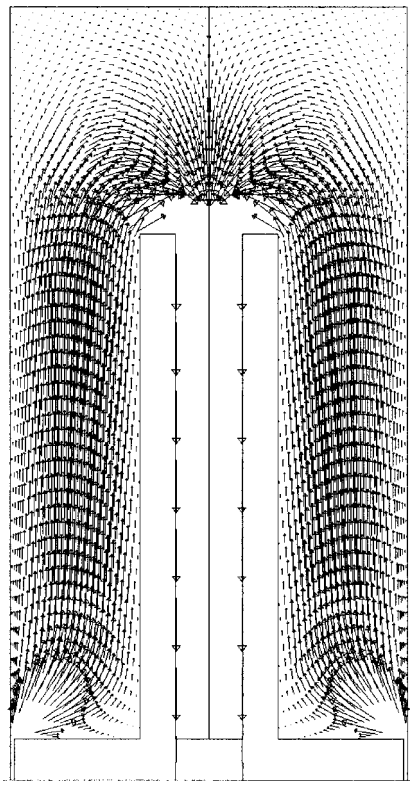

Figure 7. Flow field in NETL quartz reactors; axisymmetric; feed from narrow annulus along the perimeter of the bottom of the reactor; reactor with product withdrawal from the coaxial tube.

two *x–y* planes in Figure 8. The performance of this reactor is very similar to an ideal constant stirred-tank reactor as the RTD shows (Figure 12).

The Tingey reactor also had very high sweep efficiency (Figure 9). Small recirculation zones formed at the entrance of the annular section of the reactor, but the majority of the reactor volume was retained in this annular section where the reactor performed like a tubular laminar flow reactor. The flow of gases out of the annulus and toward the product port had small stagnant zones along the surfaces and no recirculation zones. The RTD plot (Figure 11) is representative of a laminar flow reactor with dispersion, being very close to the ideal PFR behavior.

The flow field of the Kochubei and Moin reactor (Figure 10) was similar to a laminar flow reactor. It exhibited high sweep efficiency and had no significant recirculation or stagnant zones (Figure 10). However, the broader RTD and its displacement toward lower times (Figure 11) confirms the channeling observed in the flow field at the bottom part of the reactor (Figure 10). There is a small effect of the stagnant zone as well, observed in the tailing of the RTD. It was assumed that the static mixer on the left-hand side of the reaction zone mixed the CO_2 and H_2 feed streams perfectly and instantly as they entered the reactor zone.

Despite the almost ideal behavior observed in the reactors used by Graven and Long (1954) and Tingey (1966), there was a fourfold difference in the reaction rate constants reported for these investigators, suggesting that the discrepancy was not related to the geometry of the reactor.

Conversions of the rWGSR. The influence of reactor geometry on the kinetics results was also determined by modeling the rWGSR in each reactor. The rate of reaction was determined from Eq. 9. The rate constant was obtained from Eq. 8 using the values reported in the GRI database (GRI-Mech 3.0, 2000). The reaction conditions were 1173 K, 0.1 MPa, equimolar feed of CO_2 and H_2, and a residence time of 0.5 s. The results, shown in Table 3, indicate that the outlet concentrations were within 7% of one another, confirming that the reactor geometry was not responsible for the differences observed in the reported reaction rate expressions.

Effect of pressure on the quartz reactor results

Because all prior studies had been confined to ambient pressure conditions and there was a slight difference between the NETL low-pressure and high-pressure results, the effect of elevated pressure conditions used in this study on the reaction kinetics was considered. The low-pressure experimental results of Tingey (1966) and Kochubei and Moin (1969) are in excellent agreement with the value obtained from the Bradford mechanism by using the values for the rate constant of the elementary steps reported in the GRI database (GRI-Mech 3.0, 2000) in Eq. 8: k_1, k_{-1}, and k_2, the rate constants of the initiation (Eq. 3) step, termination (Eq. 6) step, and forward

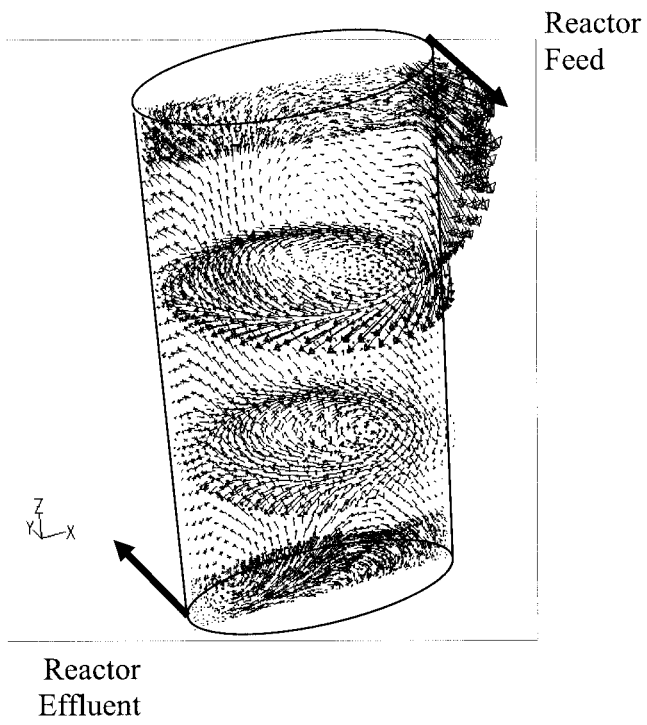

Figure 8. Graven and Long reactor; nonaxisymmetric cylindrical reactor; tangential feed entering at the top, right-hand corner of the *x–z* plane; tangential withdrawal of products through narrow tube at the bottom left-hand corner of the *x–z* plane; the two circular *x–y* cross sections are 1/3 and 2/3 of the way up the reactor in the *z*-direction.

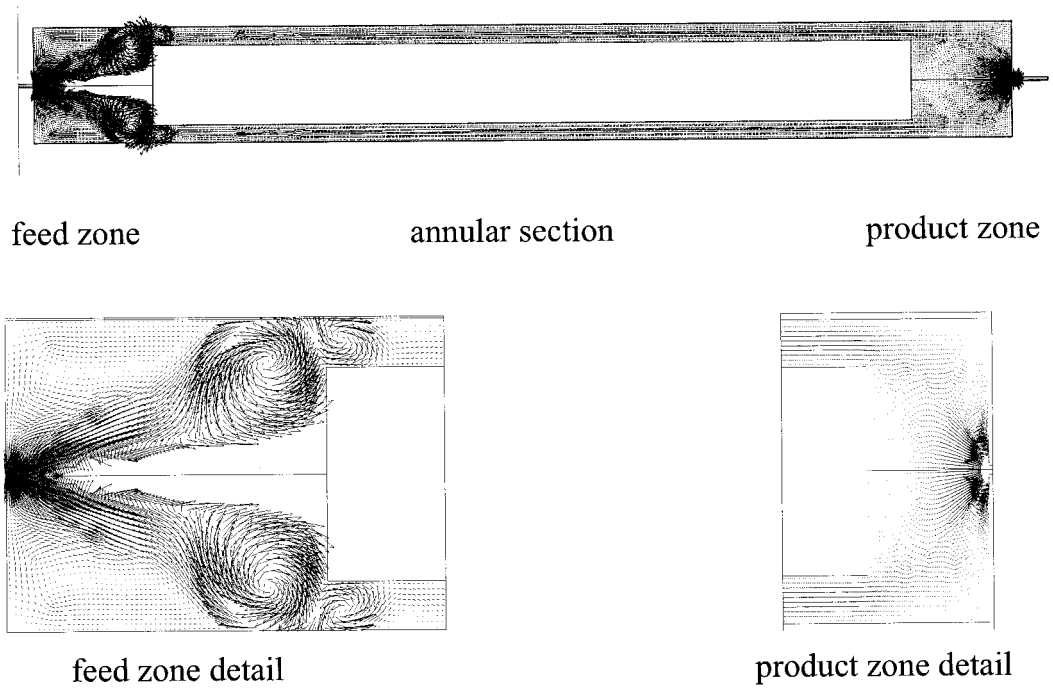

Figure 9. Tingey reactor; axisymmetric; enlargement of feed and product sections provided; white rectangle is a solid quartz cylinder; white flow field in feed section is high velocity flow field.

reaction of Eq. 4, respectively. Although Reaction 4 is known to display pressure dependency (Bierman et al., 1978; Fulle et al., 1996; Troe, 1998), with the rate constant being proportional to the total pressure, the pressure dependency is very weak (<10%) under the temperature range of interest in this study. Therefore, the very small difference between our low-pressure and high-pressure results was probably attributable to experimental uncertainties rather than to changes in the reaction mechanism. Further, the difference of the NETL results and the Kochubei and Moin (1969) and Tingey (1966) results cannot be attributed to the pressure difference.

Effect of H and OH not being at stationary state conditions within the reactor

The concentration of H and OH radicals within the reactor may not have been invariant, as was assumed in the derivation of the expression for the overall rate constant (Eq. 4). This effect was addressed to some extent in the prior investigations of the low-pressure rWGSR. Graven and Long (1954) noted an induction period for the rWGSR, a common feature in chain-

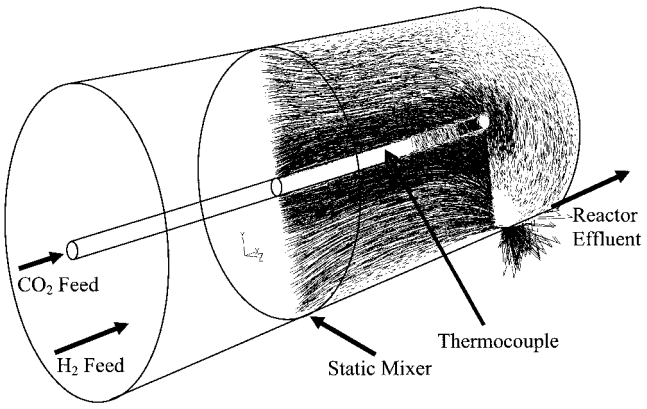

Figure 10. Kochubei and Moin reactor; nonaxisymmetric cylindrical reactor; axial feed along entire cross section on the lefthand side of the reactor.

Product withdrawn through a narrow tube at the bottom right corner of the *x–z* plane; white field in the center of the *x–z* plane is a thermocouple; velocity vectors on a *x–y* circular plane normal near the right-hand side of the reactor also shown; white field in this plane near the bottom corresponds to high fluid velocity near the exit tube.

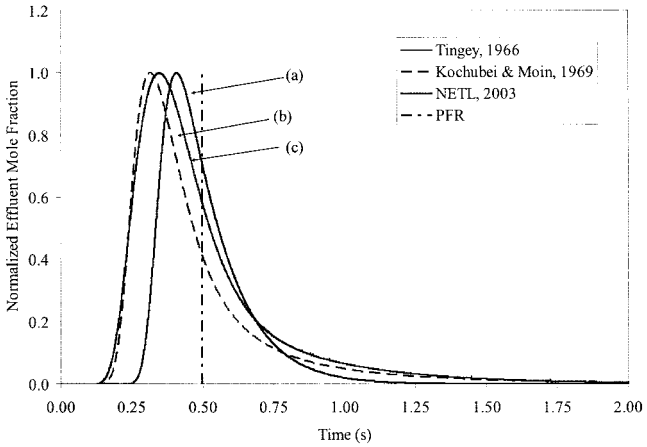

Figure 11. Residence time distribution (RTD) plots for the (a) Tingey (1966), (b) Kochubei and Moin (1969), and (c) NETL reactors.

Nominal residence time is 0.5 s. Ideal case (PFR) reactor is included as comparison.

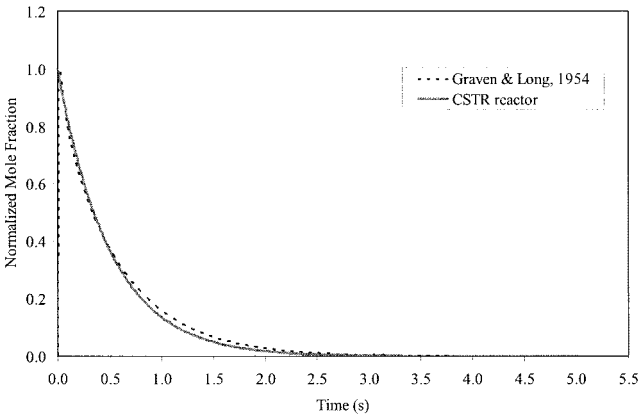

Figure 12. RTD plots. Graven and Long (1954) reactor.

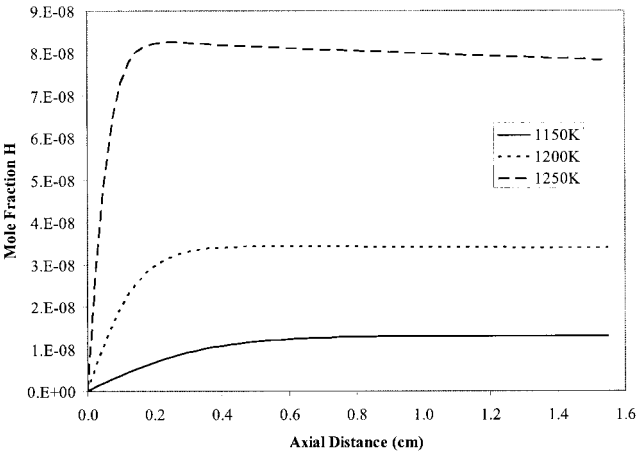

Figure 13. ChemKin® simulation of the rWGS in a tubular reactor. Inlet molar flow rates: $CO_2 = H_2 = 50$ sccm.

Reactor diameter, 1 cm. Pressure, 1.6 MPa.

reaction chemistry. Kochubei and Moin (1969) kept the H_2 stream at the reaction temperature for a time that was sufficiently long (15–1000 s) to achieve a stationary state concentration of H [i.e., the equilibrium concentration from the H_2 dissociation (Eqs. 3 and 6)] before mixing it with CO_2 at the reactor inlet. Tingey (1966) stated that the geometry of the reactor was changed to minimize the observed induction period, which was attributed to heating and cooling times as well as the time to achieve invariant concentrations of H and OH radicals within the reactor.

The possibility of changing concentrations of H and OH under our experimental conditions of rapid feed heating and mixing at the reactor entrance was studied using ChemKin®. (Chemkin® is a software for solving complex chemical kinetics problems. We used the application Creslaf, which models laminar, chemically reactive boundary layer flow in a tubular channel. The thermodynamic and transport data of all the species have either been calculated or collected from different available Web libraries.) The NETL empty quartz reactor (Figure 7) was modeled with a tubular laminar flow reactor of comparable dimensions (1 cm diameter, 1.6 cm long). The residence time of the simulations was maintained at values similar to those observed in the experiments by adjusting the volumetric flow rate. The elementary steps of the Bradford gas-phase mechanism were used as the input for ChemKin® and rate constant values were taken from the GRI database. Figure 13 shows the molar fraction of H as a function of the distance along the reactor. The simulation results indicate that the NETL results may have been influenced by the nonstationary state concentration of H, which would vary significantly along the first fourth (0–0.4 cm) of the NETL reactor (1.6 cm total length). In the temperature range corresponding to our experiments, 1148–1198 K, the steady-state concentration of H was attained only at the latter section of the reactor, confirming that the initial transient period of [H] and [OH] values must be accounted for in determining the actual rate parameters of the reaction.

The Bradford mechanism was solved numerically to determine whether this induction period might have a significant effect on the overall reaction at low conversions. Stiff integrators (ODE23s from MatLab®) were used to solve the concentration–time profiles for each one of the six species involved in the reaction mechanism. This simulation describes the reaction as it would take place in an ideal isobaric and isothermal (i.e., constant density) batch reactor. Values of the individual rate constants were taken from the GRI database. Figure 14 shows the concentration profile of H as a function of reaction time at 1250 K and 1.6 MPa, confirming the results from the ChemKin simulation. The simulation was run until a H_2 conversion of 10% was obtained, which was low enough to minimize the effect of the opposite reaction. There was a continuous increase in [H] until the stationary state value was achieved at a time $>$ 0.5 s (conversion at $t = 0.5$ s is 1.86%), suggesting that the

Table 3. CFD Conversions of the Four Reactors Assuming Identical Operating Conditions and Reaction Rate Constant*

Reactor	CO_2 Conversion, %
Graven and Long (1954)	0.0990
Tingey (1967)	0.1017
Kochubei and Moin (1969)	0.0990
NETL (this work)	0.1053

*Conditions: 1173 K, 0.1 MPa, residence time 0.5 s, inlet molar fractions of CO_2 and H_2 are 0.5.

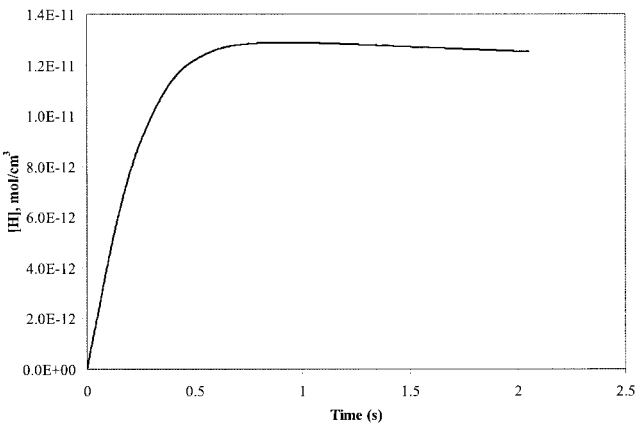

Figure 14. Concentration–time profile for H species. $[CO_2]_0 = [H_2]_0$, $[CO]_0 = [H_2O]_0 = 0$, 1250 K, 1.6 MPa, final conversion is 10%.

period during which [H] changes plays a significant role in the gas-phase kinetics, especially for low reaction times/conversions.

The reaction rate expression derived from the Bradford mechanism is

$$r = \frac{d[\mathrm{CO}]}{dt} = k_2[\mathrm{CO_2}][\mathrm{H}] - k_{-2}[\mathrm{CO}][\mathrm{OH}] \tag{18}$$

Equation 18 reduces to Eq. 7 under steady-state concentrations of H and OH. The second term on the right-hand side can be neglected for the early stages of the reaction because the concentration of CO is close to zero, k_2 and k_{-2} are of the same order of magnitude, and [OH] is several orders of magnitude smaller than [H]. The reaction rate can therefore be simplified to the following expression:

$$r = \frac{d[\mathrm{CO}]}{dt} = k_2[\mathrm{CO_2}][\mathrm{H}] \tag{19}$$

From Eq. 19 and Figure 14, it can be concluded that as the reaction commences, the rate of reaction *increases* (rather than decreases) with residence time because the increase in [H] is more significant than the decrease in $[CO_2]$. Once an invariant concentration of [H] is attained, however, the rate of reaction decreases with residence time as CO_2 is depleted.

If the reaction rate data are collected during this initial period and analyzed using Eq. 9 (the rate expression obtained under the assumption of stationary [H]), the rate constant will be given by Eq. 20 (obtained from combining Eqs. 9 and 19). This rate constant will be an *apparent* rate constant rather than the *effective* rate constant of the rWGSR (Eq. 9).

$$k = k_2 \frac{[\mathrm{H}]}{[\mathrm{H_2}]^{1/2}} \tag{20}$$

The effect of the changing concentrations of H and OH on the magnitude of the reaction rate constant was determined for conditions of 1250 K and 0.1 MPa, to provide an indication of the significance of the nonstationary state condition on the interpretation of the results. The reaction rate constant was determined using: (a) Eq. 20 and [H] and $[H_2]$ values from the simulation during the initial nonstationary period (e.g., $t <$ 0.5 s in Figure 14); (b) results from the simulation when stationary [H] is imposed at the beginning of the reaction (i.e., inlet [H] is the equilibrium value at that temperature); (c) results directly from the simulation of the Bradford mechanism where the simulation is allowed to run long enough for both the nonstationary state and stationary state regimes to be manifest, that is, until stationary state is achieved (the rate constant was determined by linear regression from runs varying the inlet $[H_2]$ and $[CO_2]$); (d) NETL experimental correlation for the rate constant obtained by analyzing our experimental rate data with Eq. 9; (e) the GRI data in Eq. 8; (f) the correlation of Tingey (1966); and (g) the correlation of Kochubei and Moin (1969). Results are presented in Table 4. The simulation results that account for the changing concentrations of H and OH, entry (b), are of the same order of magnitude as our experimental results, entry (d), suggesting that if [H] varies during an experiment but this change is not accounted for (i.e., Eq. 9 is used to solve for k), then the k values will overestimate the effective rate constant. This is a likely cause for the discrepancies between the data reported in this study and those of Tingey (1966) and Kochubei and Moin (1969). The presence of the nonstationary period where [H] has not yet attained its equilibrium value might also explain the results of Graven and Long, whose rate constant values lie between our correlation and the predicted value from the steady-state Bradford expression (Eq. 8).

An attempt to further verify that the presence of a nonstationary state regime at the reactor inlet caused an overestimation of the reaction rate constant was then made. It is well known that quartz surfaces act as radical quenchers for reactions involving H radicals. This would cause an increase in the rate of the chain termination, by the additional wall reaction. Simulations of the intrinsic kinetics (MatLab®) suggested that such an increase would bring the [H] to a stationary state earlier during the reaction. However, the value of the stationary [H] is lower than that predicted from the purely gas-phase reaction. This should render an energy of activation similar to the Bradford value, but with a smaller pre-exponential value. Such a possibility was studied using simulations (ChemKin®) and an experiment with a quartz-packed quartz reactor. The temperatures were chosen in the interval where surface reactions appear to have some effect on the rWGSR (i.e., 1073–1123 K) (Kochubei and Moin, 1969; Tingey, 1966).

We attempted to track the radical quenching effect by adding the surface reactions suggested in the work of Aghalayam (Aghalayam et al., 1998). However, the kinetic parameters available (i.e., the sticking coefficient) provide only an upper bound for the effect of radical quenching. Consequently, the simulation predicted a large inhibition in the rate of reaction even at high temperature ($>$1148 K) where such inhibition has not been observed experimentally (Graven and Long, 1954; Kochubei and Moin, 1969). Therefore, no reliable estimation could be obtained from these calculations.

Figure 15 presents the experimental results from the quartz reactor packed with small cylinders of quartz (Table 2), which increased the quartz surface area by a factor of 3. Our correlation was extrapolated to the 1123–1223 K temperature range to facilitate the comparison with our previous empty reactor results. CFD simulations of this packed reactor, in which the packing was modeled as porous media, yielded flow patterns nearly identical to those shown in Figure 7. The rate constant for the quartz-packed quartz reactor was similar to the results of Tingey (1966) and Kochubei and Moin (1969). The corresponding values of the pre-exponential constant and the energy

Table 4. Estimation of k Values at 1250 K and Atmospheric Pressure*

	Condition	k $(\mathrm{cm^3/mol})^{\gamma-1}$ $\mathrm{s^{-1}}$
a	Nonstationary [H]	325.0
b	Mixed, nonstationary and stationary [H]	79.0
c	Stationary [H]	7.1
d	NETL	44.0
e	GRI, stationary [H]	7.3
f	Tingey (1967)	9.1
g	Kochubei and Moin (1969)	9.0

* γ is the global reaction order.

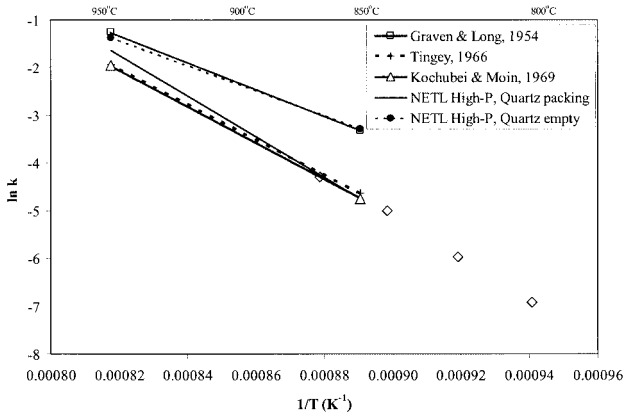

Figure 15. Arrhenius representation of rate constant for the high-pressure (1.6 MPa) rWGS reaction in the quartz packing reactor, $r = k[CO_2][H_2]^{0.5}$, k ($L^{0.5}$ $mol^{-0.5}$ s^{-1}).

The actual data points are represented by open diamonds, whereas the solid line represents their extrapolation to higher temperatures.

of activation are reported in Table 1. This observation appears to corroborate the hypothesis that the suppression or minimization of the period of the reaction where [H] increases considerably, brought by the radical-quenching effect of the quartz surface at moderate temperature, prevents an overestimation of the rate constant. However, we could not reconcile the observation of Kochubei and Moin (1969) of a small enhancement in the reaction rate brought by the addition of quartz packing. The high inlet [H] in the work of Kochubei and Moin would reduce the impact of the radical quenching, however. Further, the removal of H radicals from the gas phase could eventually drive the chain initiation step toward the production of H, decreasing the concentration of H_2.

Low-pressure rWGSR in an Inconel reactor

Rates of reactions in quartz vessels provide an understanding of the intrinsic kinetics of the rWGSR. Industrial application of this technology will occur in vessels where the reacting gases will be exposed to the metal surfaces within the reactor. Therefore, the catalytic wall effects on the rate of reaction were evaluated for empty and packed Inconel® 600 reactors at 1173 K and 0.1 MPa using an equimolar feed of CO_2 and H_2. Conversions were very high (10–40%), given the short residence time (<0.5 s) and the equilibrium limitation of 55%, as shown in Figure 16. These levels of conversion were approximately two orders of magnitude greater than those observed using the quartz reactor, which were less than 0.1% under the same experimental conditions. This result implied that the metal walls of the Inconel® 600 reactor catalyzed the reaction. An increase in the Inconel surface area was achieved by packing the reactor with Inconel rings. As shown in Figure 16, the conversions were twice that observed with the empty Inconel reactor.

High-pressure reverse water gas shift reaction in an Inconel reactor

The rWGSR was also conducted at high-pressure conditions in an Inconel reactor over a wide temperature range using equimolar feeds of CO_2 and H_2. Longer residence times were used (8–10 s) because of the increase in gas density and limitations on the maximum flow rate of the reactor effluent. The high-pressure results from the Inconel reactor experiments are presented in Figure 17 along with experimental results obtained using the empty quartz reactor. The rate of reaction in the Inconel reactor was significantly greater than that obtained in the quartz reactor, especially at low temperature. Near-equilibrium conversions were attained at temperatures > 873 K in the Inconel reactor. These results confirm the observations obtained at low-pressure conditions (Figure 16); Inconel® 600 surfaces catalyze the rWGSR. Levels of conversion were so high that accurate kinetic expressions could not be derived for the reverse WGS reaction in an Inconel reactor. Although a residence time of 10 s was used in this study, the residence time needed to achieve this level of conversion may have been substantially less, especially at higher temperature.

Both the low-pressure and high-pressure results indicated that the Inconel® 600 catalyzed the rWGSR. Two rings of the Inconel® 600 packing (72% Ni, 17% Cr, and 10% Fe) were analyzed using a scanning electron microscope equipped with an energy dispersive X-ray detector (SEM–EDS) before and after their use in the low-pressure reactor [Figure 18(a) and (b)], respectively. Significant loss of Ni and/or enrichment of Cr occurred in the Inconel surface after exposure of the Inconel to the rWGSR environment. (The Al, Si, and Ti detected in the rings reflect the composition of the Inconel® 600; the source of the Ca is not known but could be attributable to surface contamination.) A likely cause of Ni loss is the so-called metal dusting. This type of corrosion is characterized by mass loss resulting from the formation of carbon deposits in H_2–CO–H_2O environments in the temperature range 673–1073 K. The carbon diffuses into the metal and the nickel migrates to the surface, forming small pure-nickel particles. Inconel® 600 has been reported to be susceptible to this kind of attack (Klower et al., 1998). Evidence to this effect was gathered in our experiments: a considerable amount of coke was removed from the reactor and SEM–EDS analysis confirmed the presence of small Ni particles dispersed in the coke. The formation of carbon deposits may be attributable to the Boudouard reaction (Eq. 21), as a result of the somewhat large CO concentrations

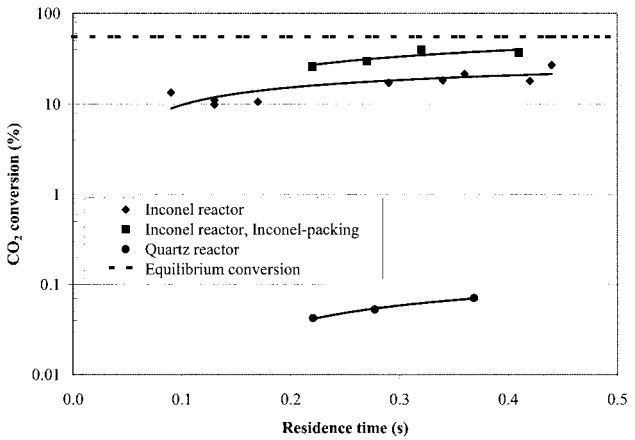

Figure 16. Reverse WGS reaction in an Inconel 600 reactor. 1173 K, 0.101 MPa, $[H_2]_0 = [CO_2]_0$.

Equilibrium conversion at these conditions is 55%.

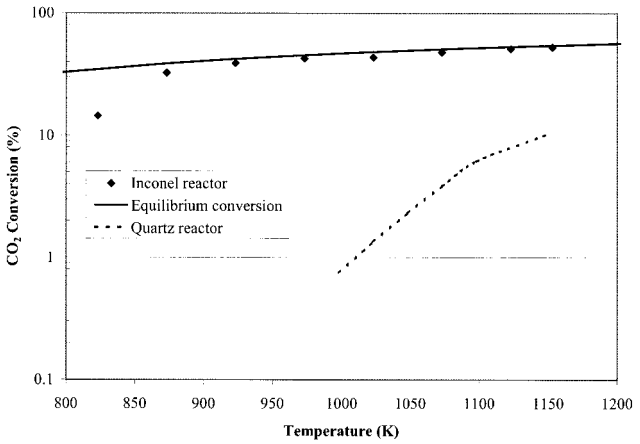

Figure 17. Reverse water–gas shift reaction in an Inconel 600 reactor. 1.6 MPa, $[H_2]_0 = [CO_2]_0$.

Conversions in the quartz reactor were estimated with our high-pressure kinetic results. Residence times were 8–10 s.

present in the system. This reaction is known to occur in the temperature range 673–1173 K.

$$2CO \leftrightarrow C + CO_2 \quad (21)$$

Although the mass loss in Inconel® 600 associated with "metal dusting" is more considerable than that for other high-Ni alloys, the damage appears to be more superficial (Baker et al., 2002). However, other materials should be considered for the long-term operation of the moderate-high temperature, high-pressure WGSR.

Another side reaction, formation of methane, was observed in the Inconel reactor. The concentration of methane at the outlet of the reactor exhibited temperature dependency reaching a maximum value at 1023 K, as shown in Figure 19. Methane formation in a $CO–CO_2–H_2–H_2O$ system is possible via reactions 22–25. With our experimental data it is not possible to determine which one of those reactions is the main contributor to the formation of methane. However, the fact that the CO/H_2O ratio decreases and the CO_2/H_2 ratio increases noticeably at 1023 K suggests that reaction 22 and/or 24 are playing an important role in the process. Removal of H_2 from the system led to complete suppression of methane formation.

$$CO + 3H_2 \leftrightarrow CH_4 + H_2O \quad (22)$$

$$CO_2 + 2H_2 \leftrightarrow CH_4 + 2H_2O \quad (23)$$

$$2CO + 2H_2 \leftrightarrow CO_2 + CH_4 \quad (24)$$

$$C + 2H_2 \leftrightarrow CH_4 \quad (25)$$

Conclusions

The rate of reaction of the homogeneous, reverse water–gas shift reaction was evaluated in an empty quartz reactor at elevated-temperature (1148–1198 K), low-pressure (0.1 MPa) conditions in the absence of a diluent gas. The power-law rate expression used exponent values of 1.0 and 0.5 for CO_2 and H_2, respectively. The reaction rate was characterized by an activation energy of 53 kcal/mol (222 kJ/mol) and a pre-exponential constant of 1.09E07 $L^{0.5}$ $mol^{-0.5}$ s^{-1}. This result was consistent with the previously published low-pressure rate expression of Graven and Long, but the resulting rates were roughly four times greater than reaction rates obtained in our quartz-packed reactor (energy of activation and pre-exponential constant were 356 kJ/mol and 3.0E14 $L^{0.5}$ $mol^{-0.5}$ s^{-1}, respectively) and rates

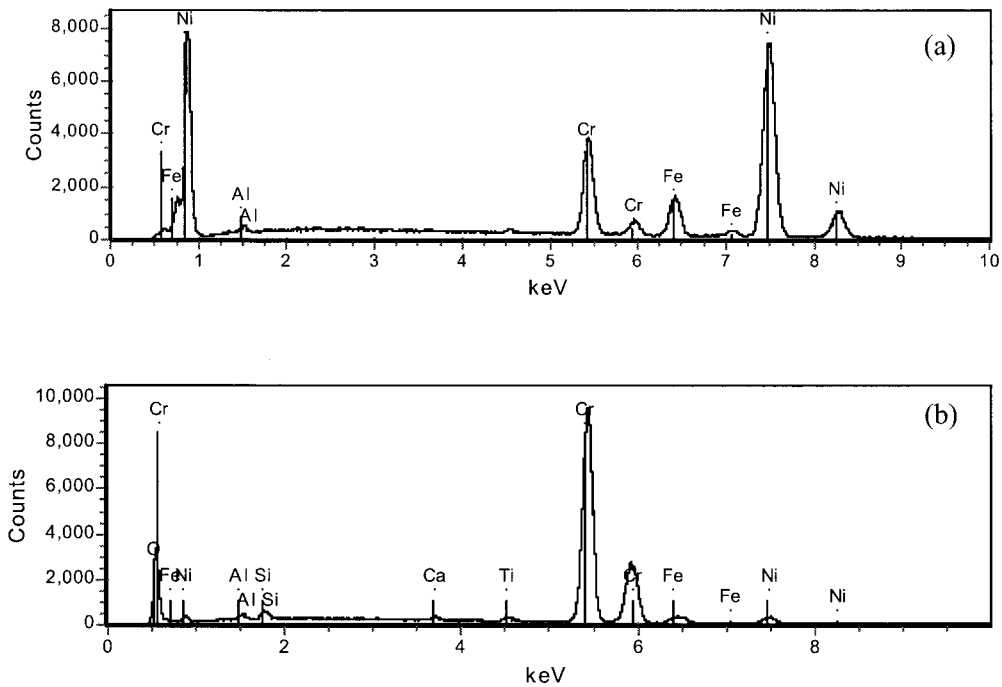

Figure 18. SEM–EDS for Inconel 600 rings before (a) and after (b) exposure to reverse WGSR environment.

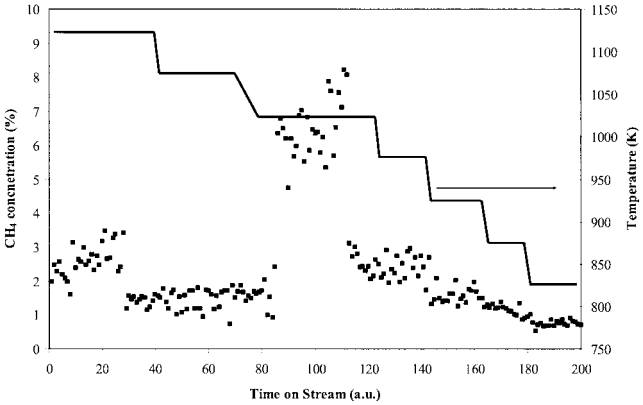

Figure 19. Side reactions in the WGS in an Inconel 600 reactor. Formation of methane as a function of temperature.

1.6 MPa, $[H_2]_0 = [CO_2]_0$. Residence times were 8–10 s.

reported by Tingey and by Kochubei and Moin. CFD simulation results indicated that differences in reactor geometry were not responsible for these differences. Further, oxygen, which is known to catalyze the reverse WGS reaction, was maintained at a concentration of less than 1 ppm in our reactor. The importance of an initial induction period in which the concentration of the chain carriers increases steadily with time was confirmed and the discrepancies between the different studies could be related to this effect. The simple gas-phase mechanism proposed by Bradford was found to satisfactorily describe the reaction. The presence of packing at moderately high temperature reduced the effect of the induction period by achieving the stationary state more quickly because of the H radical quenching in the quartz surface.

A pressure-equilibrated quartz reactor was also used to study the homogeneous rate of reaction for the first time at high temperature, high-pressure conditions (up to 1.6 MPa). The results yielded an activation energy of 52 kcal/mol (218 kJ/mol) and a pre-exponential constant of 5.99E08 $L^{0.5}$ $mol^{-0.5}$ s^{-1}. The rate constants correlated by the low-pressure and high-pressure Arrhenius expressions were in good agreement over the 1148–1198 K temperature range, indicating there was no significant effect of elevated pressure on the rate constant.

Conversions attained in an Inconel® 600 reactor at 1173 K and 0.101 MPa were approximately two orders of magnitude greater than those attained in the quartz reactor for residence times of 0.1–0.5 s. A dramatic increase in the reaction rate was also observed when the Inconel® 600 reactor was operated at high pressure, with near-equilibrium conversions realized at temperatures as low as 873 K for residence times of 8–10 s. This increase in conversion suggested that the Inconel® 600 surfaces catalyzed the rWGSR. Therefore, the use of intrinsic kinetic results based on quartz reactors in the design of a reverse WGS Inconel® 600 reactor will lead to overestimates of the volume required to attain a specified level of conversion. Further, the depletion of nickel from the Inconel® 600 reactor surfaces indicates that metal dusting is an issue that needs to be addressed in an Inconel® 600 reactor for the moderately high temperature rWGSR.

Notation

$C_{j,r}$ = molar concentration of reactant and product species j in reaction, mol/m^3
$D_{i,m}$ = diffusion coefficient for species i, m^2/s
E_a = energy of activation, kJ/mol
k = rate constant of the overall rWGSR, $(L/mol)^{0.5}$ s^{-1}
K_{eq} = equilibrium constant of the forward WGSR
k_i = rate constant of elementary reaction i ($i = 1, -1, 2, -2, 3, -3$), $(cm^3/mol)^{\gamma-1}$ s^{-1}; γ depends on the reaction
k_O = pre-exponential factor, $(L/mol)^{\gamma-1}$ s^{-1} or $(cm^3/mol)^{\gamma-1}$ s^{-1}; γ depends on the reaction
I = unit tensor
$\vec{J}_i$ = diffusive flux of species i, mol m^{-2} s^{-1}
$[M]$ = molar concentration of species M, mol/L or mol/m^3
$M_{w,i}$ = molecular weight of species i, kgmol/kg
N_R = number of the reactions
N_r = number of chemical species in reaction r
p = pressure, MPa
R_i = rate of production of species i by chemical reaction, mol m^{-3} s^{-1}
$\hat{R}_{i,r}$ = molar rate of creation/destruction of species i in reaction r, mol m^{-3} s^{-1}
r = reaction rate, mol L^{-1} s^{-1}
S_i = rate of reaction by addition from the dispersed phase plus any user-defined source, mol m^{-3} s^{-1}
T = absolute temperature, K
t = time, s
$\vec{v}$ = velocity vector, m/s
Y_i = local mass fraction of species i

Greek letters

α = reaction rate exponent for H_2
β = reaction rate exponent for CO_2
ΔH = heat of reaction, kJ/mol
γ = global reaction order
ρ = density, kg/m^3
$\bar{\bar{\tau}}$ = stress tensor
μ = molecular viscosity, Pa·s
$\nu'_{i,r}$ = stoichiometric coefficient for reactant i in reaction r
$\nu''_{i,r}$ = stoichiometric coefficient for product i in reaction r
$\eta'_{j,r}$ = forward rate exponent for each reactant and product species j in reaction r
$\eta''_{j,r}$ = backward rate exponent for each reactant and product species j in reaction r

Superscript

$\mathbf{T}$ = transposed matrix

Acknowledgments

The authors gratefully acknowledge the operational and maintenance contributions of the Parsons engineering technicians, including Ronald Hirsch, Jeremy Brannen, Ray Rokicki, Russ Miller, Brian Neel, Michael Ditillo, and Bruce Blednick. This work was sponsored through the "Transportation Fuels and Chemicals," "Gasification Technologies," and "Hydrogen, Fuel Cells, and Infrastructure" programs within the U.S. Department of Energy. F.B. acknowledges Universidad de Antioquia for granting a leave of absence to pursue his doctoral degree.

Literature Cited

Aghalayam, P., P. Bui, and D. Vlachos, "The Role of Radical Wall Quenching in Flame Stability and Wall Heat Flux: Hydrogen–Air Mixtures," *Combust. Theory Modell.,* **2**, 515 (1998).

Baker, B. A., G. D. Smith, and S. A. McCoy, "Selection of Nickel-Base Alloys for Metal Dusting Resistance," *Ammonia Technical Manual*, 257 (2002).

Barbieri, G., and F. DiMaio, "Simulation of the Methane Steam Reforming Process in a Catalytic Pd-Membrane Reactor," *Ind. Eng. Chem. Res.*, **36**, 2121 (1997).

Benson, H. E., "Processing of Gasification Products," in *Chemistry of Coal Utilization*, M. Elliot, ed., Wiley, New York, Chap. 25 (1981).
Biermann, H. W., C. Zetzsch, and F. Stuhl, "On the Pressure Dependence of the Reaction of OH with CO," *Ber. Bunsenges. Phys. Chem.*, **82**, 633 (1978).
Bradford, B. W.; "The Water–Gas Reaction in Low-Pressure Explosions," *J. Chem. Soc.*, 1557 (1933).
Enick, R. M., B. D. Morreale, J. Hill, K. S. Rothenberger, A. V. Cugini, R. V. Siriwardane, J. A. Poston, U. Balachandran, T. H. Lee; S. E. Dorris, W. J. Graham, and B. H. Howard, "Evaluation and Modeling of a High-Temperature, High-Pressure, Hydrogen Separation Membrane for Enhanced Hydrogen Production from the Water–Gas Shift Reaction," in *Advances in Hydrogen,* C.E.G. Padró and F. Lau, eds., Kluwer Academic/Plenum Publishers, New York, pp. 93–100 (2000).
Fluent, Fluent User's Guide, Fluent Incorporated, Lebanon, NH (2003).
Fogler, H. S., *Elements of Chemical Reaction Engineering*, 3rd Edition, Prentice Hall, Ann Arbor, MI (1999).
Fulle, D., H. F. Hamann, H. Hippler, and J. Troe, "High Pressure Range of Addition Reactions of OH. II. Temperature and Pressure Dependence of the Reaction HO + CO ↔ HOCO → H+ CO_2," *J. Chem. Phys.*, **105**, 983 (1996).
Graven, W. M., "Errata." *J. Am. Chem. Soc.*, **76**, 6421 (1954).
Graven, W. M., and F. J. Long, "Kinetics and Mechanisms of the Two Opposing Reactions of the Equilibrium CO + H_2O ↔ CO_2 + H_2," *J. Am. Chem. Soc*., **76**, 2602 (1954).
GRI-Mech 3.0, http://www.me.berkeley.edu/gri_mech/ (2000).
Holgate, R., and J. Tester, "Oxidation of Hydrogen and Carbon Monoxide in Sub- and Supercritical Water: Reaction Kinetics, Pathways, and Water–Density Effects. 2. Elementary Reaction Modeling," *J. Phys. Chem.* **98**, 810 (1994).
Karim, G. A., and D. Mohindra, "A Kinetic Investigation of the Water–Gas Shift Reaction in Homogeneous Systems," *J. Inst. Fuel*, 219 (1974).
Klower, J., H. J. Grabke, and E. M. Muller-Lorenz, "Metal Dusting of Nickel-Base Alloys," *Mater. Corros.*, **49**, 328 (1998).
Kochubei, V. F., and F. B. Moin, "Kinetics of the Reaction of CO_2 with Hydrogen," *Kinetika i Kataliz*, **10**, 992 (1969).
Moe, J. M., "Design of Water–Gas Shift reactors," *Chem. Eng. Progress*, **58**(3), 33 (1962).
Newsome, D., "The Water–Gas Shift Reaction," *Catal. Rev. Sci. Eng.*, **21**(2), 275 (1980).
Singh, C. P.; and D. N. Saraf, "Simulation of High-Temperature Water–Gas Shift Reactors," *Ind. Eng. Chem. Process Des. Dev.*, **16**(3), 313 (1977).
Tingey, G. L., "Kinetics of the Water–Gas Equilibrium Reaction. I. The Reaction of Carbon Dioxide with Hydrogen," *J. Phys. Chem.* **70**(5), 1406 (1966).
Troe, J., "Modeling the Temperature and Pressure Dependence of the Reaction HO + CO ↔ HOCO ↔ H+ CO_2," *Proc. Int. Symp. on Combustion*, The Combustion Institute, Pittsburgh, PA, 167 (1998).
Wender, I., "Reactions of Synthesis Gas," *Fuel Process. Technol.*, **48**, 189 (1996).

Manuscript received Dec. 17, 2002, and revision received Aug. 6, 2003.